Development of an Aerodynamic Model and Control Law Design for a High Altitude Airship

Joseph B. Mueller* and Michael A. Paluszek†
Princeton Satellite Systems, Princeton, NJ 08542

Yiyuan Zhao‡
University of Minnesota, Minneapolis, MN 55455

Lighter-than air vehicles are an attractive solution for many applications requiring a sustained airborne presence. The buoyancy force provides an energy-free form of lift, offering a non-traditional approach to long-duration missions for which traditional aircraft are not well-suited. Potential applications include roving or hovering surveillance and communication utilities for both military and commercial use, and a variety of remote-sensing instruments for the scientific community. In particular, the Missile Defense Agency plans to utilize unmanned airships at high-altitudes to provide a long-duration missile defense presence around the coast-line of the United States. Operated at 70 kft, each of these "high altitude airships" will fly above all regulated air-traffic for several months to years, will reside in a steady atmospheric regime, and will utilize solar energy to provide all required power.

Two key objectives for this type of mission are that the unmanned airship have exceptionally long endurance, and that it operate with a sufficiently high-level of autonomy. In order to achieve these objectives, a robust guidance and control system is required, capable of auto-piloting and controlling the airship under an extremely wide range of atmospheric and wind conditions. The successful design of such a system first requires an accurate model of airship dynamics across its expansive flight envelope, and a representative model of the expected disturbances.

The dynamics of an airship are markedly different from traditional aircraft, with significant effects from added mass and inertia, and a much higher sensitivity to wind. In this paper, a typical airship configuration is first sized to meet energy balance and mass constraints. The geometry of this configuration is then used to develop a general aerodynamic model for the airship. The equations of motion with added mass and inertia are developed, and the open-loop dynamics are analyzed across a range of flight conditions. Finally, control laws are designed for a single operating condition, and the closed-loop performance is presented across a range of velocities.

I. Introduction

Lighter-than-air (LTA) vehicles represent a unique and promising platform for many applications that involve a long-duration airborne presence. Achieving their lift through buoyancy, these vehicles require much less power than traditional aircraft. This opens the door to renewable sources of energy, which would enable controlled flight to be maintained indefinitely. Potential applications include roving or hovering surveillance and communication utilities for both military and commercial use, plus a variety of remote-sensing instruments for the scientific community. In particular, the Missile Defense Agency (MDA) plans to utilize unmanned airships at high altitudes to provide a long-duration missile defense presence around the coast-line of the United States. Operated at 70 thousand feet, each of these "high altitude airships" (HAA)

*Senior Technical Staff, AIAA Member, jmueller@psatellite.com
†President, AIAA Member
‡Associate Professor, Aerospace Eng. & Mechanics, AIAA Associate Fellow.

Report Documentation Page

Form Approved
OMB No. 0704-0188

1. REPORT DATE	2. REPORT TYPE	3. DATES COVERED
2004		**00-00-2004 to 00-00-2004**

4. TITLE AND SUBTITLE	5a. CONTRACT NUMBER
Developoment of an Aerodynamic Model and Control Law Design for a High Altitude Airship	5b. GRANT NUMBER
	5c. PROGRAM ELEMENT NUMBER
6. AUTHOR(S)	5d. PROJECT NUMBER
	5e. TASK NUMBER
	5f. WORK UNIT NUMBER
7. PERFORMING ORGANIZATION NAME(S) AND ADDRESS(ES) **Princeton Satellite Systems,33 Witherspoon Street,Princeton,NJ,08542**	8. PERFORMING ORGANIZATION REPORT NUMBER
9. SPONSORING/MONITORING AGENCY NAME(S) AND ADDRESS(ES)	10. SPONSOR/MONITOR'S ACRONYM(S)
	11. SPONSOR/MONITOR'S REPORT NUMBER(S)

12. DISTRIBUTION/AVAILABILITY STATEMENT
Approved for public release; distribution unlimited

13. SUPPLEMENTARY NOTES
The original document contains color images.

14. ABSTRACT
see report

15. SUBJECT TERMS

16. SECURITY CLASSIFICATION OF:			17. LIMITATION OF ABSTRACT	18. NUMBER OF PAGES	19a. NAME OF RESPONSIBLE PERSON
a. REPORT	b. ABSTRACT	c. THIS PAGE			
unclassified	**unclassified**	**unclassified**		**17**	

will fly above all regulated air-traffic for several months to years, will reside in a steady atmospheric regime, and will utilize solar energy to provide all required power.

The HAA concept has several attractive features, making it a promising solution for both government programs and commercial ventures. The large surface of the HAA lends itself to the integration of solar cells. The operational altitude is above all cloud formations, enabling direct sunlight to reach the solar cells, and it resides in a calm portion of the atmosphere where the wind speeds are relatively low. The HAA concept has several advantages over satellites as well. It can maintain a geostationary location much closer to the earth, matching both the longitude and latitude at any point on the globe. Geostationary satellites are about 1,700 times further away, and they have limited coverage for extreme north/south latitudes. Continuous coverage could be provided from low-earth orbit, but would require a constellation of satellites. In addition, the HAA has the flexibility to change its target location over time, and it may be grounded, repaired, and returned to flight at any time if necessary.

Key ingredients for success of the HAA concept, whatever the application, are that it have exceptionally long endurance, and that it operate with a sufficiently high-level of autonomy. In order to achieve these objectives, a robust guidance and control system is required, capable of auto-piloting and controlling the airship under an extremely wide range of atmospheric and wind conditions. The successful design of such a system first requires an accurate model of airship dynamics across its expansive flight envelope, and a representative model of the expected disturbances.

The dynamics of an airship are markedly different from traditional aircraft, with significant effects from added mass and inertia, and a much higher sensitivity to wind. In this paper, a typical airship configuration is first sized to meet energy balance and mass constraints. The geometry of this configuration is then used to develop a general aerodynamic model for the airship. The equations of motion with added mass and inertia are developed, and the open-loop dynamics are analyzed across a range of flight conditions. Finally, control laws are designed for a single operating condition, and the closed-loop performance and robustness is presented with respect to a range of velocities.

A. Mission Scenario

The mission scenario used in this paper is summarized in Table 1. It is consistent with the mission scenario identified by the MDA.

Table 1. Mission Scenario

	English	Metric
Altitude	70,000 kft	21.3 km
Payload	4,000 lb	1,814 kg
Power to Payload	-	15 kW
Nominal Airspeed	35 knots	18 m/s
Maximum Airspeed	90 knots	46 m/s

II. High-Level Airship Design

In general, airships fall into one of two categories: *pressurized* or *rigid*. With pressurized models, the shape of the hull is maintained by a small pressure differential between the internal lifting gas and the external atmosphere. With rigid airships, the hull is formed by a lightweight skeletal structure with a fabric skin, while the lifting gas is stored in internal "gasbags". The *Graf Zeppelin II* and the *Hindenburg* were both rigid airships. Pressure airships are sometimes made "semi-rigid" by adding a structural keel to share the bending loads generated from aerodynamic forces. In this paper, a pressurized design is assumed.

The classic airship design consists of an axisymmetric, teardrop-shaped hull with a hanging empennage (or gondola) and tail fins for stability. For the purpose of this analysis, the hull is modeled as two, axisymmetric ellipsoid halves. Each ellipsoid has the same semi-minor axis, b, but different semi-major axes, a_1 and a_2. Figure 1 on the next page shows a 2-D view of the double ellipsoid model. More complex geometries have

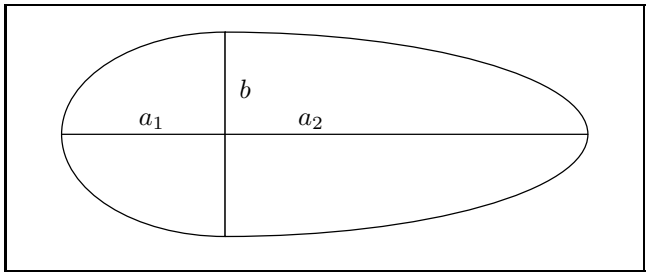

Figure 1. Double-Ellipsoid Geometry for Airship Hull

been designed with the aid of CFD tools, with the primary goals of reducing turbulence and drag.[1] Prior to the advent of CFD, however, ellipsoid geometries had historically been used to study the aerodynamics of airships. The ellipsoid configuration is therefore used in this analysis as it captures the essential aerodynamic characteristics of typical airships, while facilitating a mathematical development of the model.

The first step in the airship design process is to size the hull. The volume of the hull defines the buoyant lift capability of the airship, and determines the maximum attainable altitude. It is first necessary, however, to develop some relationships between mass, volume, and gas densities, as governed by aerostatic principles. Next, with the size and shape of the airship defined, we may compute the drag force experienced at a particular airspeed. This in turn drives the thrust and power requirements. The required coverage area for solar cells may then be analyzed, along with the mass available for structure and sub-systems. The objective of the analysis is to ensure that the proposed configuration is feasible.

A. Aerostatics of Airships

The upward buoyancy force generated by an airship is equal to the weight of the displaced air. This force is typically referred to as the "gross lift", and is defined as:

$$L_G = V_N \rho_A g \tag{1}$$

where V_N is the net volume of displaced air, ρ_A is the density of air, and g is the acceleration due to gravity. Subtracting the weight of the lifting gas (Helium), we obtain the "net lift", L_N. Noting that the volume of displaced air is equal to the volume occupied by the Helium, the equation for the net lift is:

$$L_N = V_N \left(\rho_A - \rho_H\right) g \tag{2}$$

This represents the amount of lift available to counteract the weight of the airship structure and payload.[2]

The density of both the air and Helium vary with altitude. Assuming that both gases have the same pressure and temperature, their densities change uniformly with altitude. Although a slight pressure differential is required, it is small enough to neglect for the purposes of this analysis.

As the airship rises, the density of Helium decreases along with the atmospheric density. Therefore, since the mass of the Helium remains fixed, the volume V_N must increase. This variation in internal lifting gas volume is achieved through ballonets – bags of air inside the hull which expand and contract to regulate the internal pressure (and thereby the volume). At the launching altitude (assume sea level), the density is at its highest value. The ballonets are expanded to their maximum volume, and V_N is at a minimum. As the airship begins to rise, the ambient density and pressure both fall, and air is automatically ejected from the ballonets to match the falling pressure. Clearly, at some point during the ascent, the ballonets will become completely empty. At this point, no further expansion of the lifting gas volume is possible. The net volume has reached a maximum value, V_{max}. This point is termed the "pressure altitude".

Continued ascent causes a reduction in net left as the densities fall but the volume remains constant. The pressure differential also increases, creating a *superpressure* condition, which can result in rupture of the exterior skin if the differential becomes too great. Helium may be vented to avoid rupture, but this is extremely undesirable in long-endurance applications as it reduces the available lift and shortens the mission life. It is therefore an important criteria in autonomous operations to keep the airship below the pressure altitude.

It can be shown that the net lift is constant over all altitudes, up to the pressure altitude. This is based upon the assumption that the density of the lifting gas changes at the same rate as the atmospheric density. Let ρ_{A0} be the density of air at sea level, and denote the density ratio as:

$$\sigma = \frac{\rho_{A}}{\rho_{A0}} \tag{3}$$

where ρ_{A} is the density of air at a given altitude. The density of Helium at that altitude is:

$$\rho_{H} = \sigma \rho_{A} \tag{4}$$

Noting that the net volume is equivalent to the mass of Helium divided by the density of Helium, we may rewrite Eq. 2 on the preceding page as:

$$L_N = m_{H} \left(\frac{\rho_{A0}}{\rho_{H0}} - 1 \right) g \tag{5}$$

This shows that the net lift is independent of altitude. At the pressure altitude, the net volume becomes V_{max}. Let the density ratio at this altitude be denoted by σ_p. The equations for the volume at the pressure altitude and at sea level are:

$$V_{max} = m_{H} / \left(\sigma_p \rho_{H0} \right) \qquad V_0 = m_{H} / \rho_{H0} \tag{6}$$

It follows that the volume of Helium at sea level and the maximum volume are related through σ_p.

$$V_0 = \sigma_p V_{max} \tag{7}$$

At an altitude of 70 kft, $\sigma_p = 0.061$. The net volume at sea level is therefore only 6% of the total available volume, meaning that the ballonets must occupy the remaining 94%. It will likely be difficult to realize this large of an inflation ratio. This problem may be avoided by utilizing vectored thrust and aerodynamic lift at low altitudes for climbing.

To maintain vertical equilibrium through the buoyancy force alone, the net lift must equal the combined weight of the airship structure, systems and payload.

$$L_N = \left(m_s + m_p \right) g \tag{8}$$

Here, m_s represents the mass of the structure and all systems (including power, propulsion, pressure control, etc.) and m_p represents the payload mass.

B. Sizing the Airship Hull

Given the basic aerostatic principles that govern the airship, and assuming a classic teardrop shape for the hull, it is possible to choose a set of dimensions that provide a volume suitable for a pressure airship operating at 70 kft. We first combine Eqs. 6, 5 and 8 to find the following expression:

$$V_{max} = \frac{m_s + m_p}{\sigma_p \left(\rho_{A0} - \rho_{H0} \right)} \tag{9}$$

This equation determines the total required volume of the airship hull based upon the mass of the airship structure and payload, and the density ratio (which is a function of altitude). Because the mass of the airship is dependent upon the total volume, it becomes a design challenge to maximize the volume while minimizing the structural mass. Let us break down the total structural mass as follows:

$$m_s = m_f + m_0 \tag{10}$$

where m_f is the mass of the external fabric and m_0 is the remaining mass of the airship structure and all supporting systems. The mass of the external fabric is proportional to the surface area through the fabric density, ρ_f.

$$m_f = \rho_f S \tag{11}$$

From this perspective, a spherical shape is desired as it provides maximum volume with minimum surface area. A sphere is a poor choice for the aerodynamics, however, as it generates significant pressure drag. The challenge is to develop a shape which meets the competing objectives of minimizing both the drag and the surface area.

Recall the double ellipsoid geometry of the hull (see Figure 1 on page 3). The diameter of the hull is defined as $D = 2b$, while the length is $L = a_1 + a_2$. Let us now introduce κ as the length ratio, defined as follows:

$$\kappa = \frac{a_2}{a_1} \tag{12}$$

In order to maintain the teardrop shape, the constraint of $\kappa > 1$ is imposed. An example geometry is shown in Figure 2, with $L = 250$ m, $D = 75$ m, and $\kappa = 2$. It follows that $a_1 = 83.\bar{3}$ and $a_2 = 166.\bar{6}$.

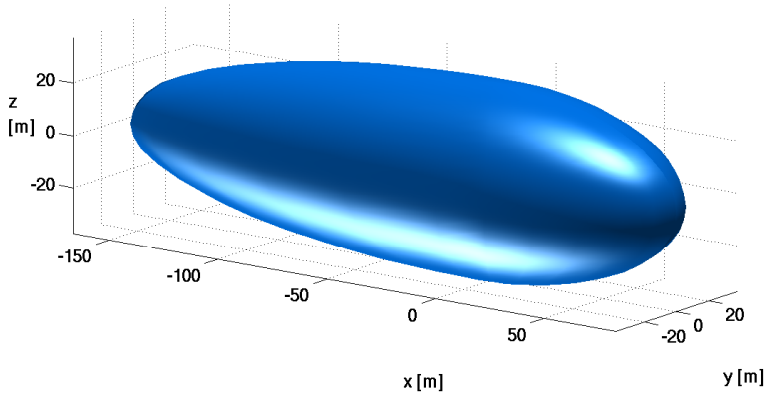

Figure 2. 3D View of Double-Ellipsoid Hull Geometry

For a given shape, we can define the ratio of the surface area over the volume as k_{sv}. The equation for maximum required volume may now be written as:

$$V_{max} = \frac{m_0 + m_p}{\sigma_p \left(\rho_{A0} - \rho H0\right) - \rho_f k_{sv}} \tag{13}$$

The volume of this geometry is 736,311 m^3, and the surface area is 48,054 m^2. This gives a value of 0.0653 for k_{sv}. Using this geometry, we may now solve for m_0 as a function of the other parameters:

$$m_0 = V_{max} \left[\sigma_p \left(\rho_{A0} - \rho_{H0}\right) - \rho_f k_{sv}\right] - m_p \tag{14}$$

This represents the mass available for the internal structure and all systems. Using the above volume and a payload mass of 4,000 lb (or 1,814 kg), Figure 3 on the next page plots several curves of m_0 as it varies with the fabric density and the surface-to-volume ratio. The blue dot indicates an available mass of 19,651 kg corresponding to a fabric density of $\rho_f = 0.5$ kg/m^2 and $k_{sv} = 0.0653$. Polyester has traditionally been the preferred fabric for airships, and has a density of 0.33 kg/m^2. However, additional coatings or films are required to reduce permeability and increase thermal insulation, which adds to the weight.

C. Drag Estimation

With the size and shape of the airship now defined, we can calculate the expected drag at the desired operating condition. The usual expression for the aerodynamic drag force on a body is given as:

$$D = \frac{1}{2}\rho U^2 A C_D \tag{15}$$

where ρ is the atmospheric density, U is the free-stream velocity, A is the reference area and C_D is the non-dimensional drag coefficient of the body. The drag on a typical airship body has significant contributions from both skin friction and pressure.

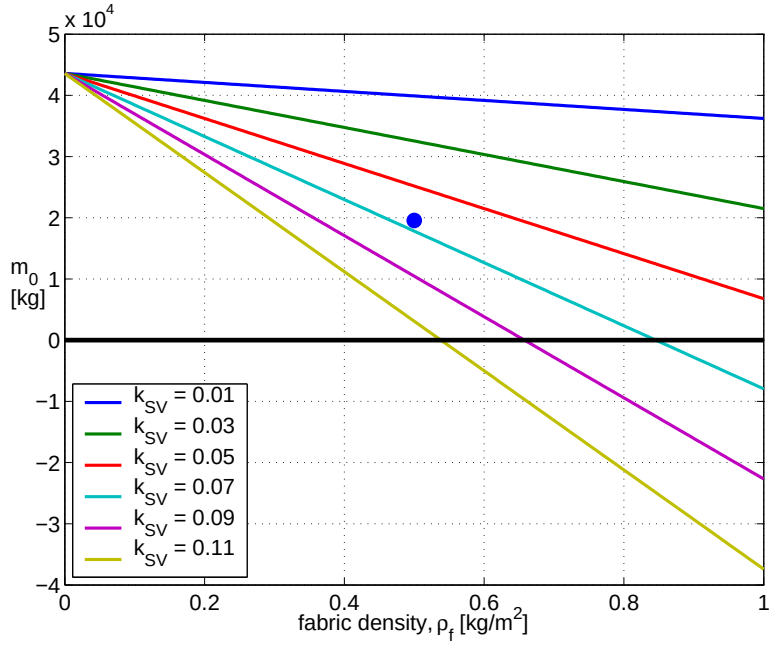

Figure 3. Mass Available for Internal Structure and Systems vs. Fabric Density

For airships, it is common practice to express the reference area in terms of the hull volume:

$$A = V^{2/3} \tag{16}$$

The drag coefficient associated with this reference area definition is provided in 2 for several values of thickness ratio. The thickness ratio is the maximum hull diameter divided by the total length. The geometry presented in Section B on page 4 has a reference area of 8,154 m^2 and a thickness ratio of 0.3. For this ratio, the analytic and experimental values of C_D are 0.0244 and 0.0255, respectively. An average value of 0.025 is chosen for subsequent analysis. If we instead use the surface area S as the reference area, the corresponding drag coefficient is 0.00424.

Consider a flight condition where the airship is at its target altitude of 70 kft, and flying at the maximum expected airspeed of 46 m/s. Using a drag coefficient of 0.025 and the given reference area, the total drag force is approximately 15.4 kN. Flying at the nominal airspeed of 18 m/s, the drag reduces to just 2.4 kN.The drag will be higher at lower altitudes, but we are interested in the nominal operating condition, where the airship spends the vast majority of its time.

D. Power Requirements

The power required by a propulsion system with efficiency η_p to apply thrust T at velocity U is given as:

$$P_{req} = \frac{TU}{\eta_p} \tag{17}$$

To maintain equilibrium, the thrust must equal the drag.

Power is generated by the solar cells during the day. It varies from zero at sunrise to a maximum value mid-day, and back to zero at sunset. The expression is given as:

$$P_{gen}(t) = SRI_{sol}(t)\eta_{sc} \tag{18}$$

where S is the total surface area of the hull, R is the percentage of the surface area covered with solar cells, I_{sol} is the solar irradiance, and $\eta_{sc} < 1$ is the solar cell efficiency. This calculation ignores the fact that the cell normals point in different directions. This may be accounted for by adjusting η_{sc} so that it reflects the

average efficiency, with directional effects included. The total energy required over a 24 hour period is found by integrating P_{req} from $t = 0$ to 24 hours. Using an average velocity $\bar{U}$ and substituting the drag in for the thrust, the result is:

$$E_{req} = \left(\frac{\rho \bar{U} S C_D}{2\eta_p} + P_0 \right) t_{day} \tag{19}$$

where P_0 represents the power required by the payload (15 kW) and t_{day} is the number of seconds in a day (left as a parameter for later manipulation). The total energy generated over a 24 hour period is found by integrating P_{req} from sunrise (t_{sr}) to sunset (t_{ss}). The variation of the solar irradiance may be approximated as a sine curve from 0 to 180 deg. The result is:

$$E_{gen} = \frac{2}{\pi} S R \eta_{sc} E_{max} \left(t_{ss} - t_{sr} \right) \tag{20}$$

where E_{max} is the peak solar irradiation occurring at mid-day. To prevent a net energy loss, the amount generated must be equal to or greater than the amount required. We may set Eq. 19 equal to Eq. 20 and solve for the minimum required solar cell coverage ratio.

$$R = \frac{\pi}{2} \left(\frac{\rho \bar{U} C_D}{2\eta_p} + \frac{P_0}{S \eta_{sc}} \right) \frac{1}{E_{max} \eta_{sc} f_{sun}} \tag{21}$$

where f_sun is the fraction of the day receiving sunlight, a parameter that varies with season and latitude.

We can compute the required solar cell coverage ratio R for a range of efficiencies. Let $f_{sun} = 0.5$, $E_{max} = 500$ W/m^2, and $P_0 = 15$ kW. We use the airship geometry from Section B on page 4, and choose an altitude of 70 kft. Two sets of curves are plotted in Figure 4, each set corresponding to a different velocity. The solid curves correspond to the maximum velocity of 46 m/s, while the dashed curves are for the nominal velocity of 18 m/s.

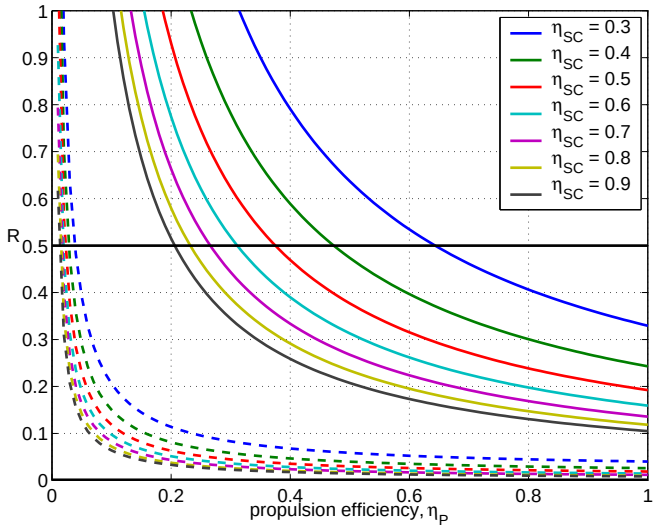

Figure 4. Required Solar Cell Coverage Ratio vs. Propulsion Efficiency

Clearly, R is physically restricted to be less than 0.5, since the solar cells must be located on the top half of the hull. The plots show that a feasible coverage ratio is possible for this geometry over a wide range of propulsion and solar cell efficiencies. A similar analysis is presented in 3.

III. Aerodynamic Model

Few publications are available which address the aerodynamic modeling of airships. A wealth of research was performed by Maxwell Munk in the 1920's and 1930's, which provided the basis for subsequent modeling

and design by others.[4,5] The aerodynamic model presented here was developed using the procedure outlined by Jones and DeLaurier.[6] This model includes expressions for axial force, normal force, and pitching moment on an axisymmetric airship hull with 4 equally sized tail fins – 2 horizontal and 2 vertical. The equations are valid for unseparated flow only.

The geometric configuration of the complete airship with fins and gondola is shown in Figure 5. It is flying at an air speed velocity of V_0 and at an angle of attack α. The sideslip angle β (not shown) is defined as a positive rotation about the z-axis, measured from the x-axis. The forces are labeled as X, Y, Z, and the moments as L, M, N. The forces and moments on the hull are evaluated from the nose to the start of the fins. Aft of this point, the hull and fins are evaluated together.

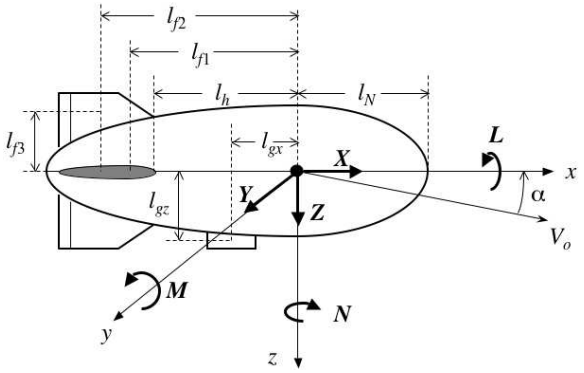

Figure 5. Steady-State Aerodynamic Model

The origin of the body frame is located at the airship's center of volume. For the double-ellipsoid geometry, the center of volume is located on the x-axis at the point:

$$x_{cv} = a_1 + \frac{3}{8}(a_2 - a_1) \tag{22}$$

where x_{cv} is measured backwards from the nose. For the airship geometry considered in this analysis, $x_{cv} = 114.58\bar{3}$. The body frame must be located at the CV location so that the added mass and inertia

Let p, q, and r denote the angular velocities about the x, y, and z axes, respectively. Let δ_{RUDT} and δ_{RUDB} indicate the deflections of the top and bottom trailing edge flaps of the rudder. Similarly, let δ_{ELVL} and δ_{ELVR} be the deflections of the left and right trailing edge flaps of the elevator. The equations for the aerodynamic forces and moments are provided below:

$$X = \frac{1}{2}\rho V_0^2 \left[C_{X1}\cos^2\alpha\cos^2\beta + C_{X2}\sin(2\alpha)\sin(\alpha/2)\right] \tag{23}$$

$$Y = \frac{1}{2}\rho V_0^2 \left[C_{Y1}\cos(\beta/2)\sin(2\beta) + C_{Y2}\sin(2\beta) + C_{Y3}\sin(\beta)\sin(|\beta|) + C_{Y4}(\delta_{RUDT} + \delta_{RUDB})\right] \tag{24}$$

$$Z = \frac{1}{2}\rho V_0^2 \left[C_{Z1}\cos(\alpha/2)\sin(2\alpha) + C_{Z2}\sin(2\alpha) + C_{Z3}\sin(\alpha)\sin(|\alpha|) + C_{Z4}(\delta_{ELVL} + \delta_{ELVR})\right] \tag{25}$$

$$L = \frac{1}{2}\rho V_0^2 \left[C_{L1}(\delta_{ELVL} - \delta_{ELVR} + \delta_{RUDB} - \delta_{RUDT}) + C_{L2}\sin(\beta)\sin(|\beta|)\right] \tag{26}$$

$$M = \frac{1}{2}\rho V_0^2 \left[C_{M1}\cos(\alpha/2)\sin(2\alpha) + C_{M2}\sin(2\alpha) + C_{M3}\sin(\alpha)\sin(|\alpha|) + C_{M4}(\delta_{ELVL} + \delta_{ELVR})\right] \tag{27}$$

$$N = \frac{1}{2}\rho V_0^2 \left[C_{N1}\cos(\beta/2)\sin(2\beta) + C_{N2}\sin(2\beta) + C_{N3}\sin(\beta)\sin(|\beta|) + C_{N4}(\delta_{ELVL} + \delta_{ELVR})\right] \tag{28}$$

$$\tag{29}$$

The coefficients are direct functions of the airship geometry. They are fully defined in the appendix. A complete aerodynamic model is available in the Aircraft Control Toolbox[a] for MATLAB.

[a] http://www.psatellite.com/products/html/ACT

IV. Equations of Motion

The standard equations of motion for a rigid body with 6 degrees of freedom are used to model the airship dynamics. In addition, the effects of added mass and inertia are included. Beginning with the standard 6 DOF equations, we have:

$$m\dot{\boldsymbol{v}} = \boldsymbol{F} \tag{30}$$

$$[I]\,\dot{\boldsymbol{\omega}} = \boldsymbol{T} \tag{31}$$

where m is the mass, $[I]$ is the inertia matrix about the center of gravity (CG), $\boldsymbol{v}$ is the linear velocity of the CG, $\boldsymbol{\omega}$ is the angular velocity of the body-fixed frame, $\boldsymbol{F}$ is the sum of all external forces, and $\boldsymbol{T}$ is the sum of all external torques. These equations are valid only with respect to an inertial reference frame.

It is convenient to express the linear and angular velocity of aircraft with respect to a body-fixed frame. To maintain generality, we define the origin of the body frame at a point that is not coincident with the CG. This is useful in cases where the CG changes slowly during flight. It also enables us to define the body frame in a way that facilitates the inclusion of added mass and inertia terms later. Thus, the equations of motion are expressed in a non-inertial, body-fixed reference frame located at an arbitrary point on the body. Figure 6 illustrates the inertial frame and the body-fixed frame on the airship. Letting $[M]$ denote the

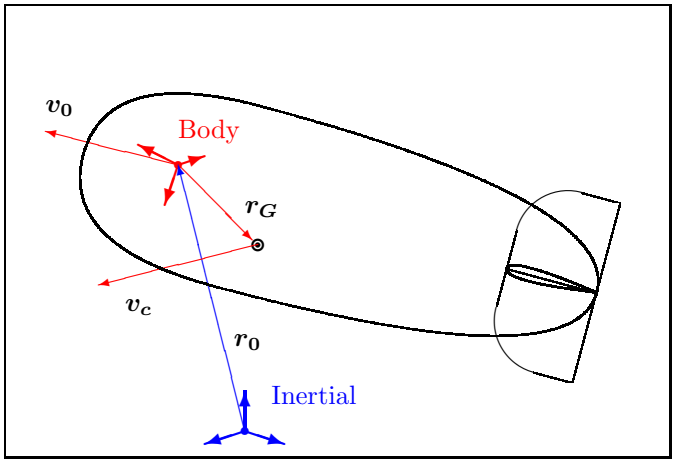

Figure 6. Coordinate Frames

transformation matrix from the inertial to body frame, the position of the CG is given as:

$$\boldsymbol{r_c} = \boldsymbol{r_0} + [M]^{\top}\,\boldsymbol{r_G} \tag{32}$$

Assuming that derivative of r_G is zero, the velocity of the CG is expressed in rotating body frame as follows:

$$\boldsymbol{v_c} = \boldsymbol{v_0} + \boldsymbol{v_{G/0}} \tag{33}$$

$$\boldsymbol{v_c} = \boldsymbol{v_0} + \boldsymbol{\omega} \times \boldsymbol{r_G} \tag{34}$$

where $\boldsymbol{v_G/0}$ indicates the velocity of the CG with respect to the origin of the body frame. Differentiating this velocity with respect to time, the translational equation of motion becomes:

$$m\left(\dot{\boldsymbol{v_0}} + \boldsymbol{\omega} \times \boldsymbol{v_0} - \boldsymbol{r_G} \times \dot{\boldsymbol{\omega}} + \boldsymbol{\omega} \times (\boldsymbol{\omega} \times \boldsymbol{r_G})\right) = \boldsymbol{F_0} \tag{35}$$

where the force $\boldsymbol{F_0}$ is defined in the body frame. The corresponding rotational equation of motion is:

$$[I_0]\,\dot{\boldsymbol{\omega}} + \boldsymbol{\omega} \times ([I_0]\,\boldsymbol{\omega}) + m\boldsymbol{r_G} \times (\dot{\boldsymbol{v_0}} + \boldsymbol{\omega} \times \boldsymbol{v_0}) = \boldsymbol{T} \tag{36}$$

where $[I_0]$ is the inertia matrix taken about the origin of the body frame. Combining Eqs. 35 and 36, we obtain the coupled nonlinear equations:

$$\begin{bmatrix} m\boldsymbol{E} & -m\boldsymbol{r_G^{\times}} \\ m\boldsymbol{r_G^{\times}} & I_0 \end{bmatrix} \begin{bmatrix} \dot{\boldsymbol{v_0}} \\ \dot{\boldsymbol{\omega}} \end{bmatrix} + \begin{bmatrix} m\left(\boldsymbol{\omega} \times \dot{\boldsymbol{v_0}} + \boldsymbol{\omega} \times (\omega \times \boldsymbol{r_G})\right) \\ \boldsymbol{\omega} \times ([I_0]\,\boldsymbol{\omega}) + m\boldsymbol{r_G} \times (\boldsymbol{\omega} \times \boldsymbol{v_0}) \end{bmatrix} = \begin{bmatrix} \boldsymbol{F_0} \\ \boldsymbol{T} \end{bmatrix} \tag{37}$$

where $\boldsymbol{E}$ is the 3×3 identity matrix, and $\boldsymbol{r}_{\boldsymbol{G}}^{\times}$ is the skew symmetric matrix of $\boldsymbol{r}_{\boldsymbol{G}}$, defined as:

$$\boldsymbol{r}_{\boldsymbol{G}}^{\times} = \begin{bmatrix} 0 & -z & y \\ z & 0 & -x \\ -y & x & 0 \end{bmatrix} \quad \text{with} \quad \boldsymbol{r}_{\boldsymbol{G}} = \begin{bmatrix} x \\ y \\ z \end{bmatrix} \tag{38}$$

and

$$\left(\boldsymbol{r}_{\boldsymbol{G}}^{\times}\right)^{\top} = -\boldsymbol{r}_{\boldsymbol{G}}^{\times} \tag{39}$$

If $\boldsymbol{r}_{\boldsymbol{G}} = 0$, then the force and moment equations decouple to give:

$$\begin{bmatrix} m\boldsymbol{E} & 0 \\ 0 & [I_0] \end{bmatrix} \begin{bmatrix} \dot{\boldsymbol{v}}_{\boldsymbol{0}} \\ \dot{\boldsymbol{\omega}} \end{bmatrix} + \begin{bmatrix} m\left(\boldsymbol{\omega} \times \boldsymbol{v}_{\boldsymbol{0}}\right) \\ I_0 \times \left([I_0]\,\boldsymbol{\omega}\right) \end{bmatrix} = \begin{bmatrix} \boldsymbol{F}_{\boldsymbol{0}} \\ \boldsymbol{T} \end{bmatrix} \tag{40}$$

which are the conventional 6 DOF equations of motion.

Any body moving through a fluid displaces that fluid. This displacement contributes to the overall change in momentum of the system. When considering the dynamics of conventional aircraft, the momentum change associated with the displaced air may be ignored, as the mass of displaced air is extremely small compared to the aircraft. For an airship, however, the mass of the air that it displaces is roughly equal to the entire mass of the vehicle. Therefore, it is necessary to account for the linear and angular momentum of the air in the equations of motion. This results in "added mass" and "added inertia" terms added to the nominal mass and inertia of the airship.

The added mass and inertia associated with the displaced fluid is added directly to the nominal mass and inertia on the left-hand side of Eq. 37 on the page before. The result is the most general form of the 6 DOF equations for a rigid body moving through a fluid:

$$\begin{bmatrix} m\boldsymbol{E} + [M'] & -m\boldsymbol{r}_{\boldsymbol{G}}^{\times} \\ m\boldsymbol{r}_{\boldsymbol{G}}^{\times} & I_0 + [I_0'] \end{bmatrix} \begin{bmatrix} \dot{\boldsymbol{v}}_{\boldsymbol{0}} \\ \dot{\boldsymbol{\omega}} \end{bmatrix} + \begin{bmatrix} m\left(\boldsymbol{\omega} \times \dot{\boldsymbol{v}}_{\boldsymbol{0}} + \boldsymbol{\omega} \times \left(\omega \times \boldsymbol{r}_{\boldsymbol{G}}\right)\right) \\ \boldsymbol{\omega} \times \left([I_0]\,\boldsymbol{\omega}\right) + m\boldsymbol{r}_{\boldsymbol{G}} \times \left(\boldsymbol{\omega} \times \boldsymbol{v}_{\boldsymbol{0}}\right) \end{bmatrix} = \begin{bmatrix} \boldsymbol{F}_{\boldsymbol{0}} \\ \boldsymbol{T} \end{bmatrix} \tag{41}$$

where $[M']$ is the added mass matrix and $[I_0']$ is the added inertia matrix.

The sum of all external forces and torques acting on the airship is expressed in the right-hand side of Eq. 41. This represents the aerodynamic forces and moments, the buoyancy, weight, and the propulsive thrust from all engines.

A. Computing the Added Mass and Inertia Matrices

The added mass and inertia matrices are functions of the vehicle shape. For the double-ellipsoid model used in this analysis, they are expressed as follows:

$$[M'] = m_{air} \begin{bmatrix} k_1 & 0 & 0 \\ 0 & k_2 & 0 \\ 0 & 0 & k_2 \end{bmatrix} \qquad [I_0'] = m_{air} \begin{bmatrix} 0 & 0 & 0 \\ 0 & k_3 & 0 \\ 0 & 0 & k_3 \end{bmatrix} \tag{42}$$

where k_1, k_2, and k_3 are ellipsoid inertia factors, found through analysis of the potential flow about the ellipsoid.[5] The added inertia matrix is defined with respect to the ellipsoid's center of volume (see Eq. 22 on page 8). The mass of displaced air, m_{air}, is found by multiplying the volume of the hull by the local atmospheric density, where the volume is given as:

$$V = \frac{2}{3}\pi\left(a_1 + a_2\right) b^2 \tag{43}$$

The inertia factors for a single axisymmetric ellipsoid are pure functions of the semi-major axis, a, and semi-minor axis, b. A complete derivation of these factors may be found in a 1926 NACA report by Tuckerman.[5] The results are repeated here for convenience. First, we define the following parameters:

$$e \;=\; \sqrt{1 - \frac{b}{a}^2} \tag{44}$$

$$f = \log\left(\frac{1+e}{1-e}\right) \tag{45}$$

$$g = \frac{1-e^2}{e^3} \tag{46}$$

$$\alpha = 2g\left(\frac{f}{2} - e\right) \tag{47}$$

$$\beta = \frac{1}{e^2} - \frac{gf}{2} \tag{48}$$

The inertia factors for this mean ellipsoid are then expressed as:

$$k_1 = -\frac{\alpha}{2-\alpha} \tag{49}$$

$$k_2 = -\frac{\beta}{2-\beta} \tag{50}$$

$$k_3 = -\frac{1}{5} \times \frac{\left(b^2-a^2\right)(\alpha-\beta)}{2\left(b^2-a^2\right)+\left(b^2+a^2\right)(\beta-\alpha)} \tag{51}$$

Here, we define a as the mean value of a_1 and a_2 from the double-ellipsoid hull model.

V. Open-Loop Dynamics

The open-loop dynamics are naturally decoupled into two modes: longitudinal and lateral-directional. Separate control are developed for each mode. The longitudinal mode consists of the following states:

- q – Pitch rate
- u – Axial velocity
- w – Normal velocity

These states are affected by the following three controls:

- τ – Throttle
- μ – Propeller pitch angle
- δ_{ELV} – Symmetric elevator deflection

The lateral-directional mode consists of the following states:

- p – Roll rate
- r – Yaw rate
- v – Lateral velocity

These states are affected by only two controls:

- δ_{RUD} – Symmetric rudder deflection
- δ_{AIL} – Differential elevator and rudder deflection (termed "aileron" deflection for convenience)

Linear models of both modes are obtained directly from the non-linear model by application of the central value theorem. The velocity components of the linear models are treated as perturbations about the trim velocity. Before the linearization may be conducted, the trim control settings must be computed. Conditions for trim flight are discussed in Section A on the following page.

Consider the airship in level flight at 21 km altitude, flying at an airspeed of 15 m/s. The linear models at this flight condition are:

$$A_{lon} = \begin{bmatrix} 0.0132 & -3.1\times10^{-5} & -4.7\times10^{-4} \\ 0 & -0.0042 & 0 \\ 7.079 & -5.9\times10^{-4} & -0.0497 \end{bmatrix} \qquad B_{lon} = \begin{bmatrix} 0.0036 & 1.1\times10^{4} & -0.0030 \\ 0.4737 & 0.0139 & 0 \\ 0.0672 & -0.0208 & -0.0574 \end{bmatrix}$$

$$A_{lat} = \begin{bmatrix} -1.6\times10^{-9} & 2.1\times10^{-10} & -2.2\times10^{-13} \\ -1.3\times10^{-11} & 0.0131 & 4.7\times10^{-4} \\ -3.0\times10^{-9} & -7.079 & -0.0497 \end{bmatrix} \quad B_{lat} = \begin{bmatrix} 0.0130 & 0.0260 \\ 0.0030 & 0 \\ -0.0574 & 0 \end{bmatrix} \tag{52}$$

This model corresponds to the geometry discussed in Section B on page 4. The weight is set equal to the buoyancy, and the CG is coincident with the CB.

A. Conditions for Trim Flight

The airship is in trim flight when the net forces and moments sum to zero. This includes contributions from the aerodynamics, gravity, buoyancy, and thrust. Three control effectors are used to establish trim flight: symmetric elevator deflection (δ_{ELV}), throttle ($\tau \in [0,1]$), and propeller pitch angle (μ). The propeller pitch angle is used for thrust-vectoring, where the propellers are rotated about the y-axis of the airship. We assume two identical propellers are mounted on opposite sides of the gondola, and that they are rotated together. The equations for longitudinal trim flight are:

$$\sum M_y = z_p T_x + x_p T_y + \bar{q} C_{M4} \delta_{ELV} + M_y^{AD} + M_y^{AS} = 0 \tag{53}$$

$$\sum F_x = T_x + F_x^{AD} + F_x^{AS} = 0 \tag{54}$$

$$\sum F_z = -T_z + \bar{q} C_{Z4} \delta_{ELV} + F_x^{AD} + F_x^{AS} \tag{55}$$

where x_p and z_p are the coordinates of each propeller, T_x and T_z are the axial and normal forces from the total propeller thrust, and $\bar{q}$ is the dynamic pressure. The aerodynamic coefficients C_{M4} and C_{Z4} are defined in the appendix. The superscripts AD and AS refer to aerodynamic and aerostatic, respectively. The aerodynamic terms are computed from the aerodynamic model, and the aerostatic terms are found to be:

$$M_y^{AS} = (B - mg)\left[(z_B - z_G)\sin(\theta+\alpha) + (x_B - x_G)\cos(\theta+\alpha)\right] \tag{56}$$

$$F_x^{AS} = (B - mg)\sin(\theta+\alpha) \tag{57}$$

$$F_z^{AS} = (B - mg)\cos(\theta+\alpha) \tag{58}$$

where B is the buoyancy force, mg is the weight, $< x_B, z_B >$ are the coordinates of the center of buoyancy (CB), and $< x_G, z_G >$ are the coordinates of the center of gravity (CG). Clearly, if the buoyancy equals the weight, and if the CG and CG are coincident, then there exist no aerostatic forces.

Let T_{max} be the maximum achievable thrust for each propeller. The axial and normal thrust values are then defined as:

$$T_x = 2\tau T_{max}\cos\mu \qquad T_z = 2\tau T_{max}\sin\mu \tag{59}$$

The solution for trim control settings is readily found by treating T_x, T_z and δ_{ELV} as the unknowns in Eqs. 56 to 58, and solving the 3×3 matrix inverse. The analytic solution is:

$$T_x = -\left(F_x^{AD} + F_x^{AS}\right) \tag{60}$$

$$T_z = kC_{Z4}\left[z_p\left(F_x^{AD} + F_x^{AS}\right) - \left(M_y^{AD} + M_y^{AS}\right)\right] + kC_{M4}\left(F_z^{AD} + F_z^{AS}\right) \tag{61}$$

$$\delta_{ELV} = \frac{k}{2\bar{q}}\left[z_p\left(F_x^{AD} + F_x^{AS}\right) - x_p\left(F_z^{AD} + F_z^{AS}\right) - \left(M_y^{AD} + M_y^{AS}\right)\right] \tag{62}$$

where the parameter k is defined as:

$$k = \frac{1}{C_{M4} + x_p C_{Z4}} \tag{63}$$

With T_x and T_z known, the resulting solutions for the propeller pitch angle and throttle are found from Eq. 59 on the preceding page.

Eq. 62 on the page before shows that the magnitude of the elevator deflection is inversely proportional to the dynamic pressure, $\bar{q}$. Since the aerodynamic forces and moments are directly proportional to $\bar{q}$, it cancels on these terms, but it remains on the aerostatic terms. As the velocity is decreased, $\bar{q}$ approaches zero. Thus, if the aerostatic forces and moments are non-zero, the required elevator deflection becomes sensitive to the following quantity:

$$z_p F_x^{AS} - x_p F_z^{AS} - M_y^{AS} \tag{64}$$

It becomes worthwhile in the design stage to minimize this quantity through careful selection of the CG, CB and propeller location.

VI. Control Law Design

An integrated guidance and control system has been designed for the high altitude airship. The overall architecture of the system is shown in Figure 7. A remote operator commands the target latitude, longitude and altitude for the airship. This information is provided to a Trajectory Planner module, which also receives the measured latitude, longitude and altitude, and other possible data, such as the estimated wind velocity. The Trajectory Planner periodically performs online trajectory optimization to generate a time-tagged trajectory sequence for the control law to follow.[7] The trajectory consists of heading angle ψ, flight path angle θ, and absolute velocity V.

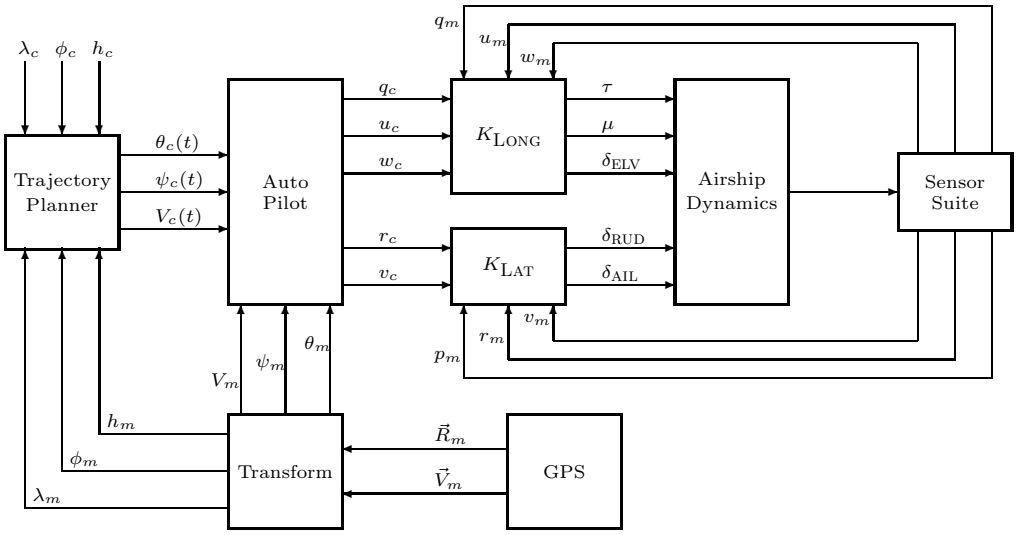

Figure 7. Control System Block Diagram

The m and c subscripts distinguish the measured and commanded signals.

A simple control law design provides robust feedback control of the airship's angular rates and velocity. The design flight condition is straight and level flight at the target altitude of 21 km, and at the nominal airspeed of 18 m/s. Based upon the analysis of the plant input matrix for each mode, separate controllers were designed for the following loops:

- **Longitudinal Mode:**
  - u -to- τ
  - u -to- μ
  - q -to- δ_{ELV}
- **Lateral-Directional Mode:**
  - r -to- δ_{RUD}

– v -to- δ_{RUD}

– p -to- δ_{AIL}

The controller for each loop is a PID with rate roll-off. The transfer function has the form:

$$K(s) = \frac{as^2 + bs + c}{s(s + 0.1)} \tag{65}$$

where a, b, and c are directly related to the proportional, integral and derivative terms of a standard PID controller. These coefficients were chosen for each loop through an iterative process, in which the robustness margins and the time response were evaluated, until the desired performance was achieved. The standard military robustness requirements (45 deg phase margin, 6 dB gain margin) are met in each loop.

A simulation of the complete non-linear model is conducted with the controllers implemented at 1 Hz. Perfect measurements and actuation are assumed. The airship is initialized at the design altitude, flying at 24 m/s with a 2 degree angle-of-attack and a 1 -degree sideslip. The desired velocity is 25 m/s, with zero angle-of-attack and sideslip. The time-response is shown in Figure 8. Even though this airspeed is far from the speed for which the controllers were designed, they still provide good performance. The augmented response is much faster than that of the open-loop system, and all of the actuators stay well within their physical limits.

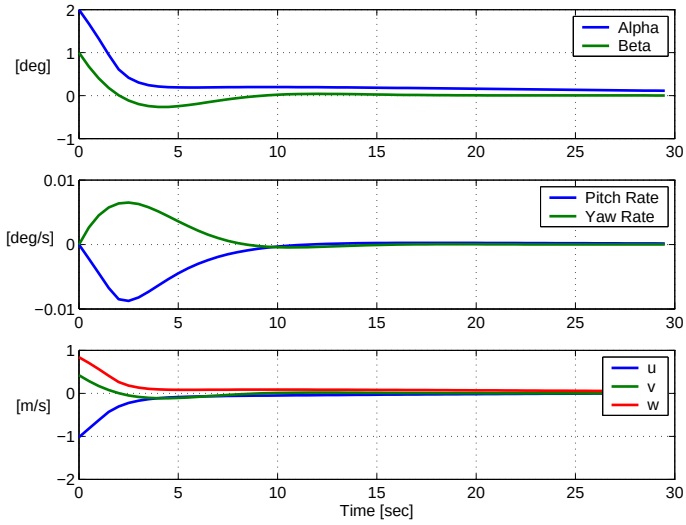

Figure 8. Time Response of Closed-Loop System

It is interesting to examine the closed-loop stability afforded by this single control law across a range of flight conditions. In this case, we vary the airspeed from 1 to 25 m/s, keeping the altitude constant at 21.3 km. The root locus for the both the longitudinal and lateral-directional modes is shown in Figure 9 on the following page. The direction of increasing velocity is denoted by increasing marker size. In each system, the dominant closed-loop poles approach the imaginary axis as the velocity decreases, signifying a reduction in stability.

The airship design considered in this analysis is statically neutral. The buoyancy equals the weight, and the two forces act at the same point. So, in the absence of aerodynamic forces, the vehicle will simply hover. This agrees with the pole locations approaching the imaginary axis at zero velocity. If the center of buoyancy is different from the center of gravity, which is likely in a real system, the vehicle would be statically unstable. A minimum amount of airspeed would be required in order to maintain stability.

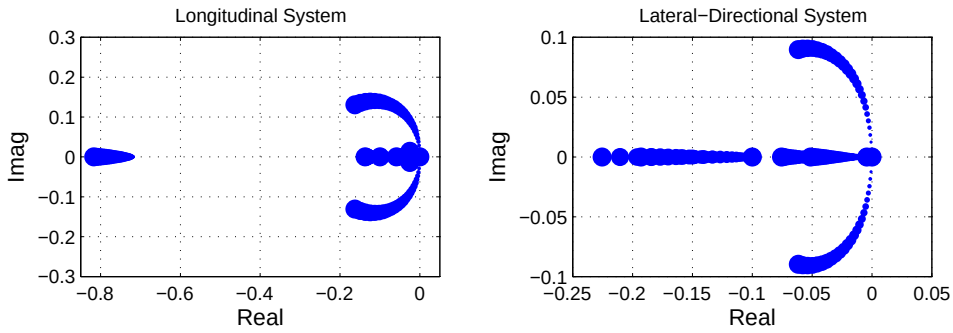

Figure 9. Root Locus of Closed-Loop Systems at Various Airspeeds

VII. Conclusions

This paper has provided useful methods for the modeling and control of a typical airship configuration, and discussed the unique issues associated with the operation of airships at high altitudes. A series of steps for sizing the airship hull were presented, based on the principles of aerostatics and daily energy balance constraints. A steady-state aerodynamic model was provided, based on the model by Jones.[6] The dynamics of the airship in flight was then expressed using the six degree of freedom equations of a rigid body with an offset CG, and including the effects of added mass and inertia. Linearized models of the open-loop dynamics were then used to develop classical, SISO controllers for tracking desired angular rates and linear velocity. The approach has shown that useful models of airship dynamics may be readily developed and analyzed. For example, the model developed in this paper has been used in the development of trajectory optimization algorithms.[7]

Future research on this topic should address the issue of model validation. High-fidelity models of airships may be obtained with the aid of CFD tools or wind-tunnel testing. However, these methods are prone to high cost and long development cycles. If the dynamics can be modeled with sufficient accuracy using an analytic approach, then multiple designs and analyses may be carried out rapidly at low cost. A particular issue important to high-altitude airships is the extensive flight envelope that they must traverse – altitudes range from sea-level to over 20 km, and airspeed velocities fluctuate strongly with the wind. It is therefore important to understand the dynamics across this entire envelope, and to assess the robustness and performance capabilities with respect to wind. It appears that this problem lends itself well to modern, robust control methods. The development of MIMO controllers using $\mathcal{H}_\infty$ and μ-synthesis techniques, for example, would offer robustness guarantees in the face of uncertain dynamics.

Appendix

The force and moment equations defined in Section III on page 7 contain 20 aerodynamic coefficients. Each of these coefficients is defined below:

$$C_{X1} = -\left[C_{Dh_0} S_h + C_{Df_0} S_f + C_{Dg_0} S_g\right] \tag{66}$$

$$C_{X2} = \left(k_2 - k_1\right) \eta_k I_1 S_h \tag{67}$$

$$= C_{Y1} = C_{Z1} \tag{68}$$

$$C_{Y2} = -\frac{1}{2}\left(\frac{\partial C_L}{\partial \alpha}\right)_f S_f \eta_f \tag{69}$$

$$= C_{Z2} \tag{70}$$

$$C_{Y3} = -\left[C_{Dch} J_1 S_h + C_{Dcf} S_f + C_{Dcg} S_g\right] \tag{71}$$

$$C_{Y4} = -\frac{1}{2}\left(\frac{\partial C_L}{\partial \delta}\right)_f S_f \eta_f \tag{72}$$

$$= C_{Z4} \quad (73)$$

$$C_{Z3} = -\left[C_{Dch} J_1 S_h + C_{Dcf} S_f\right] \quad (74)$$

$$C_{L1} = \left(\frac{\partial C_L}{\partial \delta}\right)_f S_f \eta_f l_{f3} \quad (75)$$

$$C_{L2} = -C_{Dcg} S_g l_{gz} \quad (76)$$

$$C_{M1} = -\left(k_1 - k_2\right) \eta_k I_3 S_h L \quad (77)$$

$$C_{M2} = -\frac{1}{2}\left(\frac{\partial C_L}{\partial \alpha}\right)_f S_f \eta_f l_{f1} \quad (78)$$

$$C_{M3} = -\left[C_{Dch} J_2 S_h L + C_{Dcf} S_f l_{f2}\right] \quad (79)$$

$$C_{M4} = -\frac{1}{2}\left(\frac{\partial C_L}{\partial \delta}\right)_f S_f \eta_f l_{f1} \quad (80)$$

$$C_{Nj} = -C_{Mj} \quad (81)$$

The following table defines all of the parameters appearing in the coefficient equations (Eq. 66 on the preceding page to Eq. 81).

Table 2. Definition of Parameters in the Aerodynamic Coefficient Equations

Parameter	Definition	Value
C_{Dh_0}	Hull zero-incidence drag coefficient	0.025
C_{Df_0}	Fin zero-incidence drag coefficient	0.006
C_{Dg_0}	Gondola zero-incidence drag coefficient	0.01
C_{Dch}	Hull cross-flow drag coefficient	0.5
C_{Dcf}	Fins cross-flow drag coefficient	1.0
C_{Dcg}	Gondola cross-flow drag coefficient	1.0
$\left(\frac{\partial C_L}{\partial \alpha}\right)_f$	Derivative of fin lift-coefficient with respect to the angle-of-attack at zero incidence	5.73
$\left(\frac{\partial C_L}{\partial \delta}\right)_f$	Derivative of fin lift-coefficient with respect to the flap deflection angle	1.24
S_h	Hull reference area, $V^{2/3}$	8154 m^2
S_f	Fin reference area	3656 m^2
S_g	Gondola reference area	202 m^2
l_{f1}	x-distance from origin to aerodynamic center of fins	117.5 m
l_{f2}	x-distance from origin to geometric center of fins	129.7 m
l_{f3}	y, z-distance from origin to aerodynamic center of fins	18.3 m
l_{gx}	x-distance from origin to aerodynamic center of fins	29.2 m
l_{gz}	z-distance from origin to aerodynamic center of fins	40.0 m
η_f	Fin efficiency factor accounting for the effect of the hull on the fins	0.29
η_k	Hull efficiency factor accounting for the effect of the fins on the hull	1.19
I_1	$\frac{1}{S_h}\int_{-a_1}^{a_2} \frac{dA}{dx} dx$	0.33
I_3	$\frac{1}{S_h l_h}\int_{-a_1}^{a_2} x\frac{dA(x)}{dx} dx$	-0.69
J_1	$\frac{1}{S_h}\int_{-a_1}^{a_2} 2r(x) dx$	1.31
J_2	$\frac{1}{S_h l_h}\int_{-a_1}^{a_2} 2r(x) x dx$	0.53

The lift and drag coefficients were approximated based upon the shape of the various components. Data from the NACA 1412 airfoil was used for the fins. The gondola is assumed to be stream-lined, with a cross-sectional area larger than its frontal area. See Figure 5 on page 8 for an illustration of the geometry.

Using the double ellipsoid geometry, the solution to the integrals are:

$$I_1 = \pi \frac{b^2}{V^{2/3}} \left(1 - f^2\right) \tag{82}$$

$$I_3 = \pi \frac{b^2}{3LV^{2/3}} \left(a_1 - 2a_2 f^3 - 3a_1 f^2\right) - \frac{x_{cv}}{L} I_1 \tag{83}$$

$$J_1 = \frac{b}{2V^{2/3}} \left(a_1 \pi/2 + a_2 \sqrt{1 - f^2} f + 2a_2 \sin^{-1}(f)\right) \tag{84}$$

$$J_2 = J_1 \frac{a_1 - x_{cv}}{L} + \frac{2b}{3LV^{2/3}} \left(a_2^2 - a_1^2 - a_2^2 \left(1 - f^2\right)^{3/2}\right) \tag{85}$$

where $f = (l_h - a_1)/a_2$, l_h is the length of the hull up to the leading edge of the fins, and x_{cv} is defined in Eq. 22 on page 8.

Acknowledgments

This work was performed under Phase I SBIR funding through the Missile Defense Agency, contract number HQ0006-03-C-0141.

References

[1]Lutz, T. and Wagner, S., "Drag Reduction and Shape Optimization of Airship Bodies," *Institute for Aerodynamics and Gas Dynamics, University of Stuttgart*, AIAA, Germany, 1997.

[2]Khoury, G. A. and Gillett, J. D., *Airship Technology*, Cambridge Aerospace Series: 10, 1999.

[3]Rehmet, M. A., Krplin, B., Epperlein, F., R.Kornmann, and Schubert, R., "Recent Developments on High Altitude Platforms," http://www.isd.uni-stuttgart.de/lotte/halp/paper/paper.htm.

[4]Tuckerman, L. B., "Notes on Aerodynamic Forces on Airship Hulls," Naca report no. 129, 1923.

[5]Tuckerman, L. B., "Inertia Factors of Ellipsoids for use in Airship Design," Naca report no. 210, 1926.

[6]Jones, S. P. and DeLaurier, J. D., "Aerodynamic Estimation Techniques for Aerostats and Airships," *AIAA Lighter-than-Air Systems Conference*, AIAA, Annapolis, MD, 1981.

[7]Zhao, Y., Garrard, W., and Mueller, J. B., "Bennefits of Trajectory Optimization for Airship Flights," *AIAA Unmanned Unlimited Conference*, AIAA, Chicago, IL, 2004.